A Discussion on the Differences Between the Cyclic Spectral Correlation and Coherence for Cyclostationarity-Based Condition Monitoring

Kayacan Kestel[1], Cédric Peeters[2], Jérôme Antoni[3], Quentin Léclere[4], François Girardin[5], Robert Brijder[6] and Jan Helsen[7]

[1,2,7] *Vrije Universiteit Brussel - VUB, Department of Applied Mechanics, Elsene, Brussels, 1050, Belgium*
kayacan.kestel@vub.be
cedric.peeters@vub.be
jan.helsen@vub.be

[3,4,5] *Univ Lyon, INSA Lyon, LVA, EA677, 69621 Villeurbanne, France*
jerome.antoni@insa-lyon.fr
quentin.leclere@insa-lyon.fr
francois.girardin@insa-lyon.fr

[6] *Flanders Make, Corelab DecisionS, 3920 Lommel, Belgium*
robert.brijder@flandersmake.be

ABSTRACT

Vibration signals measured on rotating machinery typically exhibit cyclostationarity due to the inherent nature of real-world rotating vibration sources. Hence, the development of signal processing tools devoted to investigating or exploiting this cyclostationarity for condition monitoring purposes of gears and bearings has seen a significant increase in research interest. One of the main approaches to analyze a vibration signal's cyclostationary behavior is the cyclic spectral correlation and its normalized derivative, the cyclic spectral coherence. Even though these two methods are closely related, they do offer different statistical insights which may influence the fault detection and trending capabilities of these tools. The aim of this work is to investigate the performance of these two methods with regard to the accuracy of tracking mechanical degradation over time. The normalization of the spectral coherence, which makes it independent of the signal power spectrum, improves the interpretability of the resulting coherence spectrum but it may lead to suppress or equalize fault-related frequency bands relative to other frequency bands and it may skew the coherence spectrum amplitudes of fault harmonics in different operating regimes for complex machinery. Tracking the evolution of a second-order cyclostationary component over time might thus be hindered by this normalization, which can lead to issues when combining such a tool with a data-driven machine learning technique that employs the operating conditions for making the cyclostationary indicators operating condition independent. Instead, using the cyclic spectral correlation, which is not normalized, may provide a more accurate depiction of the degradation process. This paper investigates whether there is any significant benefit to using the cyclic spectral correlation over the cyclic spectral coherence for monitoring complex rotating machinery and if so, when it makes sense to prefer one over the other. To answer these questions, both simulated and experimental vibration data is examined in order to highlight the differences between the two concepts.

1. INTRODUCTION

Vibration-based health monitoring tools have been developed over decades in order to track patterns related to a faulty component, to distinguish signals measured on a *healthy* machine from a *damaged* one. Tracking the statistical properties of vibration signals or investigating their spectral components in the frequency domain are two common methods utilized to assess machine health conditions. An exhaustive review of vibration-based condition monitoring techniques can be found in (Randall, 2021). Nowadays, cyclostationarity which is inherently embedded in vibration signals measured on rotating machines is often exploited for fault detection purposes. While cyclostationarity is a broad term in the signal processing domain, second-order cyclostationarity is the main order of interest in vibration-based condition monitor-

ing of rotating machinery. In an early study, several examples of signal processing techniques on second-order cyclostationary vibrations signals are demonstrated in detail (McCormick & Nandi, 1998).

Second-order cyclostationary signals exhibit periodic second-order statistics, in other words, they have periodic autocorrelation functions. An example of a second-order cyclostationary signal is the vibration emitted by a rolling element bearing fault with a crack on one of its races. Such a bearing fault generates impulses which are convolved with the resonance frequency of the structure. The repetition frequency of the pulses forms the envelope of the signal, hence, the fault detection can be made by investigating the envelope spectrum (McFadden & Smith, 1984). While the envelope spectrum, by definition, is obtained from the Fourier transform of the envelope of the signal which is estimated from its analytic signal, the spectral correlation offers another solution to estimate the envelope spectrum of the signal (Randall, Antoni, & Chobsaard, 2001). It is called the enhanced envelope spectrum (EES) and its estimation is explained in the following section. Methods based on spectral correlation are important not only as they provide an estimation of the envelope spectrum, but also because they provide frequency bands that contain the carrier frequencies.

An early comprehensive study stating that the second-order statistics in a time-series can be extracted using spectral correlation function is introduced by Gardner (Gardner, 1986). It is mentioned that signals with second-order statistics are prevalent in several mechanical systems as well as in nature, and, furthermore, a second-order periodic phenomenon only exists if the correlation between the spectral content is repeated for every cyclic frequency α. Gardner also proposed the definition of spectral coherence derived from the spectral correlation function as the strength of the second-order periodicity. The utilization of spectral correlation, nevertheless, did not become very popular until two decades ago. Randall et al. studied the application of spectral correlation density maps to the diagnosis of bearing fault on experimental vibration signals (Randall et al., 2001). It is postulated that the 2D cyclic spectral correlation density maps provide information on the bearing fault frequency in the discrete cyclic frequency α domain. Randall et al. also proposed the abovementioned enhanced envelope spectra that are estimated by integrating the cyclic spectral correlation density maps over the continuous carrier frequency f domain. It is also claimed in the same study that cyclic spectral correlation density maps help to decide on the best band-pass filter frequencies to reveal the modulation embedded in the vibration signals measured on complex machines.

Several ways of estimating the cyclic spectrum are studied and compared extensively by Antoni (Antoni, 2007) and the outcome stresses that while cyclic spectral analysis provides more insight into the vibration signals, it is not strictly more difficult to perform than conventional spectral analysis. The drawback in the use of the cyclic spectrum is that it requires the estimation of discrete modulation frequency α to an unknown upper limit, which is computationally expensive (Randall et al., 2001). In order to tackle this, a fast algorithm is proposed to estimate the cyclic spectral correlation or coherence maps employing the short-time Fourier transform (Antoni, Xin, & Hamzaoui, 2017). The diagnostic performance of spectral correlation density and spectral coherence maps is compared in (Antoni, 2009). It is shown that weak second-order cyclostationary signatures masked by strong first-order cyclostationary spectral components can be enhanced in coherence maps thanks to the normalization. Key aspects in the literature regarding the drawbacks and benefits of using spectral correlation-based vibration signal analysis for vibration-based health monitoring are briefly mentioned.

An emerging aspect in prognostics and health monitoring is also the remaining useful life (RUL) prediction, which requires robust tools to trend the health status of the machine or its distinct components. Given that the leading cause of the rotating machine failure is bearing faults (Graney & Starry, 2012), tracking the bearing fault degradation becomes critical in the evaluation of the RUL. A review of the framework extending from the development of the health indicators to inference of the RUL of the machine is made by Want et al. (Wang, Tsui, & Miao, 2018). However, it seems that there is a gap in the literature regarding a comparative study of the performance of cyclic spectral correlation map based-indicators. Within this context, two strong tools extensively utilized for bearing fault detection, namely cyclic spectral correlation and cyclic spectral coherence, are compared with regard to the accuracy of trending mechanical degradation of a roller bearing fault. Lately in the literature, cyclic spectral coherence metrics are prevalently used due to the normalization which makes the coherence spectrum bounded and improves its interpretability. Nonetheless, the normalization may mask the fault-related frequency bands relative to other frequencies, which may hinder the trending these bands.

In this paper, we compare the two methods in their ability to track mechanical degradation of a roller bearing fault. Because of the normalization and bounds of the cyclic spectral coherence, it is argued that the amplitudes of the enhanced envelope spectrum converge to a maximum value, and therefore may be less informative to assess the continuous degradation of a rolling element bearing fault. On the other hand, amplitudes of the EES obtained from the spectral cyclic correlation map are expected to be ever-increasing to the point where the point defect transforms into a distributed one. Hence, trending the amplitudes from the cyclic spectral correlation map potentially provides more information about the degradation severity of the fault. This can be particularly important when this information is used to feed a machine learning algorithm

to infer the RUL of a mechanical component of a complex rotating machine.

2. METHODOLOGY

In this section, the mathematical background regarding the estimation of the cyclic spectral correlation and coherence maps as well as the EES is given. In addition, the details of the signal simulations are explained.

2.1. The Estimation of the Cyclic Spectral Maps

For a discrete signal $x(t)$, the autocorrelation function C_{xx} can be written as (Randall et al., 2001):

$$C_{xx}(t,\tau) = \mathbb{E}\{x(t+\tau/2)x(t-\tau/2)^*\} \tag{1}$$

where $\mathbb{E}$ represents the expected value, τ is the time shift for the autocorrelation function, and the asterisk is used to show the complex conjugate.

By definition, the 2D Fourier transformation of the instantaneous autocorrelation function for both t and τ gives the spectral correlation. As the signal $x(t)$ is discrete, the spectral correlation is estimated using the discrete Fourier transformation, which is as follows:

$$\begin{aligned} SCor^{\alpha}(f) &= \lim_{\Delta T\to+\infty} \frac{1}{\Delta T} \sum_{m=-\Delta T/2}^{\Delta T/2} C_{xx} e^{-j2\pi f \frac{m}{F_s}} \\ \tau &= \frac{m}{F_s} \end{aligned} \tag{2}$$

where ΔT is the time span of the discrete Fourier transform, F_s is the sampling rate, and f carrier frequency which is spaced apart by the discrete cyclic frequency α (Gardner, 1986; Antoni, 2009). The cyclic spectral correlation density $SCor$ defined in Eq. 2 is defined for each α component which is also the counterpart of τ in the frequency domain.

Cyclic spectral coherence is also the normalized derivative of $SCor$ and is defined as:

$$SCoh^{\alpha}(f) = \frac{SCor^{\alpha}(f)}{\sqrt{SCor^{0}(f+\alpha/2)SCor^{0}(f-\alpha/2)}} \tag{3}$$

Both $SCoh$ and $SCor$ provide a two-dimensional map of the carrier and the cyclic frequencies. The cyclic frequencies give information about the modulations of the signal while the carrier frequencies represent the dominant frequency of the modulated phenomenon. Therefore, in practice, the former corresponds to the theoretical fault frequency and the latter is the resonance frequency.

As proposed in (Randall et al., 2001), the EES can be obtained by integrating the cyclic spectral correlation or cyclic spectral coherence maps over the carrier frequencies. The EES obtained from $SCor$ and $SCoh$ are estimated as follows:

$$S_{xx}^{Cor}(\alpha) = \lim_{\Delta f\to-\infty} \sum_{f=f_1}^{f_2} SCor^{\alpha}(f)\Delta f \tag{4}$$

and

$$S_{xx}^{Coh}(\alpha) = \lim_{\Delta f\to-\infty} \sum_{f=f_1}^{f_2} SCoh^{\alpha}(f)\Delta f \tag{5}$$

respectively.

2.2. Signal Simulations

In order to track the degradation of a bearing fault in time, the sum of the EES amplitudes in the vicinity of the theoretical fault frequency is used. Let $SCor\,ind$ and $SCoh\,ind$ represent the indicators estimated over the enhanced envelope spectra of $S_{xx}^{Cor}(\alpha)$ and $S_{xx}^{Coh}(\alpha)$, respectively. It must be noted that the increase of the $SCor\,ind$ over time is significantly larger than the $SCoh\,ind$, thus, the former is shown on a logarithmic scale in all the graphs.

Both simulated and experimental vibration signals are examined to test which of $SCor\,ind$ and $SCoh\,ind$ reflect the continuous degradation of a bearing fault most accurately over time, particularly for severe fault states. Signals with periodic impulses are generated and convolved with an impulse response function. White noise is added to vary the signal-to-noise ratio (SNR) from -20 dB to 30 dB in order to compare the trend of the indicators at various SNR levels. Figure 1 shows two signals with an SNR of 10 dB and -10 dB.

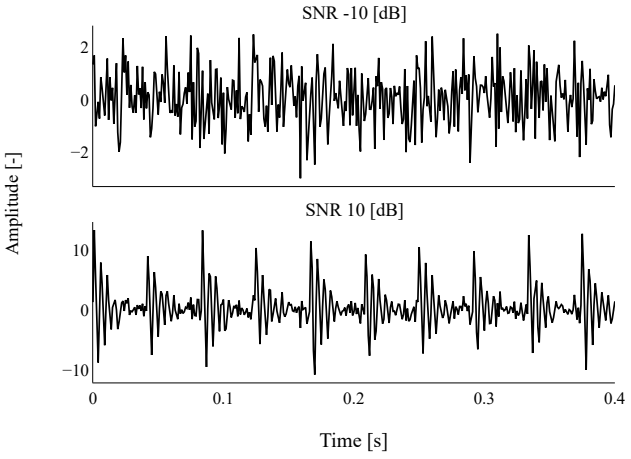

Figure 1. Simulated signals with an SNR of -10 dB and 10 dB in the time domain

The impulse repetition frequency is set to 24 Hz, therefore, frequency bins in the vicinity of that frequency and its second

harmonic are tracked over the envelope spectra. Accordingly, the sum of the amplitudes of the frequency bins corresponding to the first and second harmonics of the 24 Hz are estimated for the envelope spectra obtained using both $SCor$ and $SCoh$ and shown in Fig. 2.

The trends in Fig. 2 depict a significant difference between the indicators estimated on $SCoh$ and $SCor$ at high SNR levels. After the SNR level of 16 dB, shown with the dashed line, the increase of the $SCoh\,ind$ stagnates and the indicator tends to converge to a maximum value. This converging trend may indicate that the degradation of the simulated bearing fault also slows down. However, this is not a valid conclusion because rising SNR levels represent the degradation of the bearing fault. On the other hand, the indicator estimated on $SCor$ is ever-increasing even beyond the dashed line, which provides a better assessment of the degradation of the bearing fault.

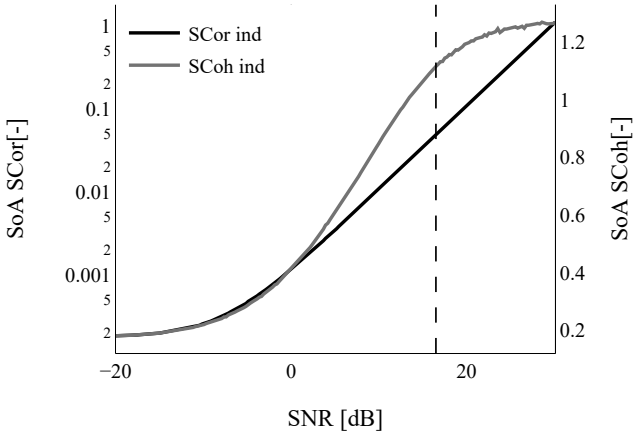

Figure 2. Evolutions of the indicators estimated on the simulated signals.

To elaborate, a machine learning algorithm trained with such a dataset may be deceived and not observe the continuous degradation of the fault at high SNR levels if the inference of the RUL is made based on $SCoh\,ind$. On the other hand, the ever-increasing trend of $SCor\,ind$ reflects the machine degradation over time as the increasing SNR represents the further degradation of the bearing fault.

Since the results obtained from the simulated signals support the stated argument that $SCor\,ind$ can provide a better assessment of the health status of a faulty bearing than $SCoh\,ind$, further investigations are performed on the experimental signals.

3. RESULTS

On the grounds of the results shown in Fig. 2, the claimed argument is further tested on the vibration signals measured on an experimental test rig. The datasets are acquired by Flanders Make, yet not publicly available.

3.1. Experimental signals

Each dataset is comprised of one second long signals sampled at 50 kHz. Run-to-failure tests are initiated with Rockwell-C indentation of 100 kg in the bearing inner race of the bearing 6205-C-TVH manufactured by FAG and the BPFI order is estimated as 5.41. Vibration signal acquisitions are made at the constant rotation speed of 2000 rpm. Three sample signals displayed in Fig. 3 demonstrate the degradation of the bearing fault over the entire run-to-failure test. The noisy signal transforms into a highly impulsive one near the end of the run-to-failure test. It must be noted that the time signal with the severe fault shown in Fig. 3 contains 33 distinct peaks, which is different than the BPFI order. This phenomenon occurs because of the significantly strong applied force to accelerate the degradation of the bearing fault. The extreme radial load leads to strong impulses only in the load zone and noise outside of it, which repeats at the shaft rotating speed of 33.3 Hz.

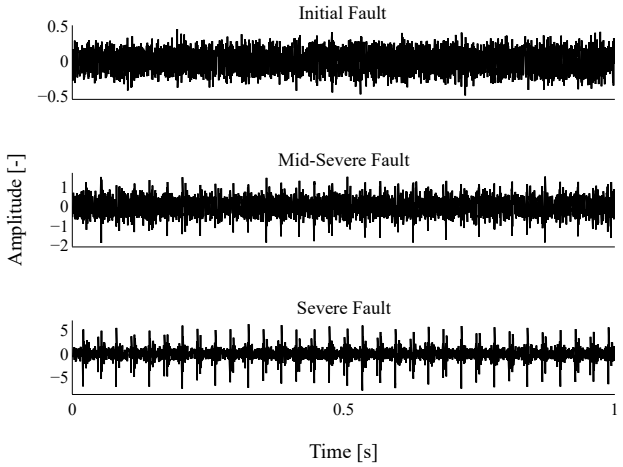

Figure 3. Experimental vibration signals in timewave form at different severity of the bearing faults.

Among 20 datasets investigated for this study, we present representative datasets. For the sake of brevity, the datasets are numbered from 1 to 4. For instance, Fig. 3 is generated using signals chosen from dataset 4. As in the figures shown for the simulated signals, the sum of amplitudes corresponding to the frequency bins in the vicinity of the theoretical BPFI frequency is estimated over the enhanced envelope spectra obtained using cyclic spectral correlation and coherence maps. The horizontal axes of Figures 4, 5, 6, and 7 represent the measurement number and early measurements are not displayed as they contain no information with regard to the degradation of the fault.

The trend of the indicators estimated for dataset 1 is shown

in Fig. 4. Both $SCor$ and $SCoh$ indicators demonstrate an overall increasing trend, except for the late measurements, where the fault appears to become distributed and the amplitudes around the BPFI frequency drop compared to the early measurements. Moreover, the $SCoh$ indicator slightly drops around measurement 1350 and elevates quickly, which does not imply any information regarding the degradation of the fault, as a self-healing of the fault is not expected. Nonetheless, a notable aspect of $SCor\,ind$ is its monotonously increasing trend. Over the degradation period of the bearing fault, the $SCor\,ind$ demonstrates a persistent behaviour. There are several other datasets which reveal a similar scenario that are not shown for the sake of brevity.

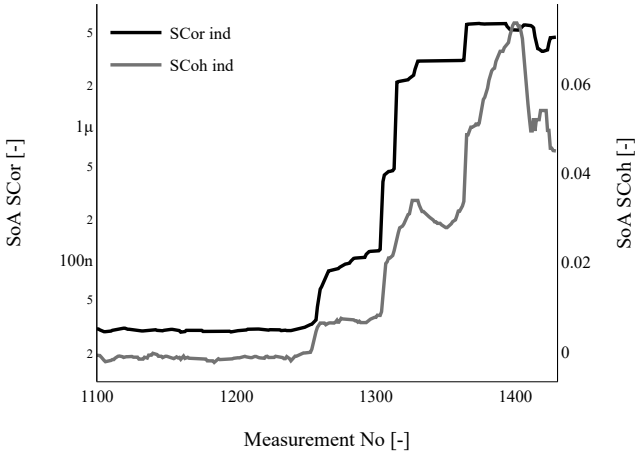

Figure 4. Evolutions of the indicators on dataset 1

Figure 5 demonstrates a different story where the trend of the $SCor$ indicator provides more information over time for the degradation of the bearing fault. The trend of the $SCor$ indicator monotonously increases and the trend is smooth over time. On the other hand, the $SCoh$ indicator exhibit spurious increases and decreases which impair the continuous assessment of the degradation of the bearing fault.

The third scenario is shown in Fig. 6. The monotonously increasing trend in $SCor\,ind$ is observed along with sudden jumps and flat regions. This behaviour of the indicator over time does not directly reflect the expected continuous degradation of the bearing fault, given the extreme load and continuous operation. Likewise, $SCoh\,ind$ exhibits steep rises. On the other hand, a gradual decline in the trend of $SCoh\,ind$ is observed just after reaching near its maximum value. This may be deceptive with regard to the inference of the state of the bearing fault. Because the decay in the trend of the indicator can be deduced as a self-healing of the fault, despite that it is unlikely.

The last figure, which in fact is representative of the majority of the investigated datasets, is demonstrated in Fig. 7. In this case, both indicators follow a similar and increasing trend

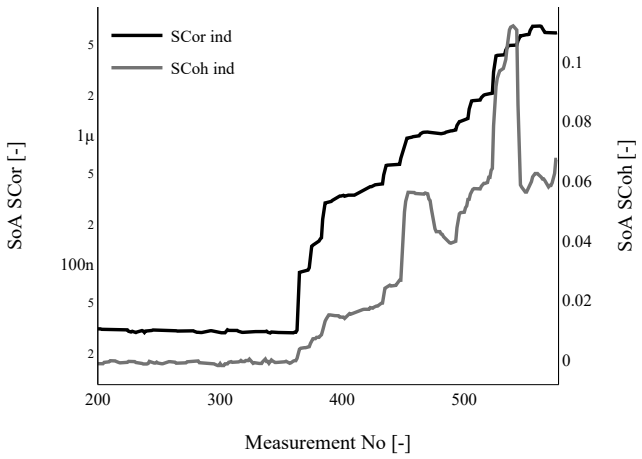

Figure 5. Evolutions of the indicators on dataset 2

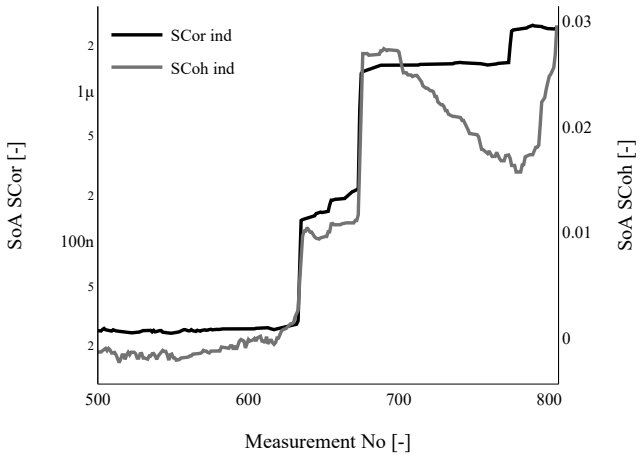

Figure 6. Evolutions of the indicators on dataset 3

without any significant spurious drops or peaks that smear the overall trend of the degradation.

Given the trends of the indicators shown in Figures 4 to 7, a convergence of the $SCoh$ indicator to a maximum value is not observed. Likewise, an ever-increasing trend for $SCor$ indicator is also absent. However, the $SCor\,ind$ maintains the monotonicity of its increasing trend to the point where the bearings fail, which offers a more convenient way of discerning the stages of the faults. Although this is not exactly the argument as showcased by the simulated signals, it is notable that the cyclic spectral correlation indicator is able to provide information regarding the degradation of bearing faults over time more clearly than the coherence-based indicator, as deterioration of the bearing faults is expected to be continuous.

The discussion regarding the trends shown in the figures is not aiming to compare the early detection or diagnosis capability of the cyclic spectral correlation and coherence. Yet it

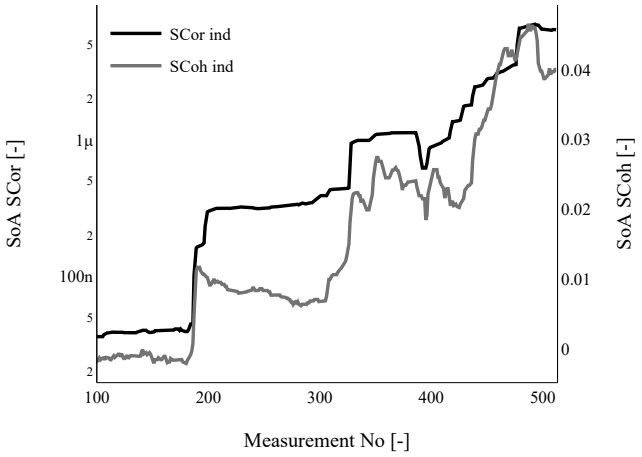

Figure 7. Evolutions of the indicators on dataset 4

is to comprehend how informative the trends of the indicators are to assess the severity of the bearing fault as this is vital information for data-driven approaches that use these indicators. Therefore, the trends of the indicators are inspected with regard to the accuracy of tracking mechanical degradation. Apart from that, the normalization of the cyclic spectral coherence makes it insensitive to the operating conditions of the machine. Therefore, as an extent of the study, these two approaches can be also tested on vibration signals measured on rotating machines operating at varying conditions.

4. CONCLUSION

The outcome of this study demonstrates that, while the simulated data shows an ever-increasing trend of the indicators estimated over the cyclic spectral correlation maps, this same phenomenon is not observed on the experimental signals. It appears that in practice the signal-to-noise ratio level after which the trend of the spectral coherence indicator converges, is not attainable on real vibration signals. This study does not aim to compare the two approaches for their superiority in terms of early fault detection. The results do indicate that the trends of $SCor\,ind$ estimated on the experimental data are monotonously increasing. On the other hand, the cyclic spectral coherence indicator does not demonstrate such a persistent trend.

The foundation of the claimed argument is that tracking the amplitude evolution in the vicinity of the theoretical fault frequency over the cyclic spectral correlations maps provides potentially more information on the degradation level of the bearing fault compared to tracking that of the cyclic spectral coherence maps. Therefore, the remaining useful life may be inferred utilizing $SCor$ in a more efficient way. Although it is not as clear as the outcome of the simulation results, the experimental results also show that $SCor\,ind$ is a relatively better tool for RUL inference thanks to its monotonicity. On the other hand, it is also demonstrated that in practice the SNR level after which the $SCoh\,ind$ converges to a maximum value is not attainable. Inspections made on 20 run-to-failure tests manifest that roller bearings fail much earlier than the required SNR level for $SCoh\,ind$ to flatten out. However, the monotonicity in the increasing trends of $SCor\,ind$ reveals that the use of cyclic spectral correlation maps come to the fore as it provides more robust information to assess the state of a bearing fault degradation continuously. Therefore, the $SCor\,ind$ appears to be a better-suited tool for data-driven approaches that try to infer the condition or the RUL of bearings based on vibration measurements.

ACKNOWLEDGMENT

This research received funding from the Flemish Government under the "Onderzoeksprogramma Artificiële Intelligentie (AI) Vlaanderen" program. The authors would like to acknowledge FWO (Fonds Wetenschappelijk Onderzoek) for their support through the post-doctoral grant of Cedric Peeters (1282221N) and SBO project Robustify (S006119N).

NOMENCLATURE

C_{xx}	autocorrelation function
f	carrier frequency
α	cyclic frequency
$SCoh$	cyclic spectral coherence
$SCoh\,ind$	cyclic spectral coherence indicator
$SCor$	cyclic spectral correlation
$SCor\,ind$	cyclic spectral correlation indicator
EES	enhanced envelope spectrum
S_{xx}^{Coh}	enhanced envelope from coherence maps
S_{xx}^{Cor}	enhanced envelope from correlation maps
RUL	remaining useful life
SNR	signal-to-noise ratio
SoA	sum of amplitudes

REFERENCES

Antoni, J. (2007). Cyclic spectral analysis in practice. *Mechanical Systems and Signal Processing*, *21*(2), 597-630.

Antoni, J. (2009). Cyclostationarity by examples. *Mechanical Systems and Signal Processing*, *23*(4), 987-1036.

Antoni, J., Xin, G., & Hamzaoui, N. (2017). Fast computation of the spectral correlation. *Mechanical Systems and Signal Processing*, *92*, 248-277.

Gardner, W. A. (1986). The spectral correlation theory of cyclostationary time-series. *Signal Processing*, *11*(1), 13-36.

Graney, B. P., & Starry, K. (2012). Rolling element bearing analysis. *Materials Evaluation*, *70*(1), 78.

McCormick, A. C., & Nandi, A. K. (1998). Cyclostationarity in rotating machine vibrations. *Mechanical Systems*

and Signal Processing, *12*(2), 225-242.

McFadden, P. D., & Smith, J. D. (1984). Vibration monitoring of rolling element bearings by the high-frequency resonance technique — a review. *Tribology International*, *17*(1), 3-10.

Randall, R. B. (2021). *Vibration-based condition monitoring: industrial, automotive and aerospace applications*. John Wiley & Sons.

Randall, R. B., Antoni, J., & Chobsaard, S. (2001). The relationship between spectral correlation and envelope analysis in the diagnostics of bearing faults and other cyclostationary machine signals. *Mechanical Systems and Signal Processing*, *5*(5), 945-962.

Wang, D., Tsui, K.-L., & Miao, Q. (2018). Prognostics and health management: A review of vibration based bearing and gear health indicators. *IEEE Access*, *6*(6), 665-676.